Iranian Journal of Microbiology

Volume 18 Number 5 (October 2026) 841-860
DOI: http://doi.org/10.18502/ijm.v18i5.22875

ORIGINAL ARTICLE

A multi-epitope-based DNA vaccine confers cross-protection against influenza A H1N1 and H3N2 viruses

Khabat Barkhordari[1], Farhad Rezaei[1*], Vahid Salimi[1], Kaveh Sadeghi[2], Mostafa Alavi Moghadam[3], Hossein Bagheri[4], Masoumeh Pourjabali[5], Maryam Karimi[6], Omid Fotouhi[7], Talat Mokhtari Azad[1*]

[1]Department of Virology, School of Public Health, Tehran University of Medical Sciences, Tehran, Iran
[2]Department of Microbiology, School of Medicine, Tehran University of Medical Sciences, Tehran, Iran
[3]Department of Emergency Medicine, Imam Hossein Hospital, Faculty of Medicine, Shahid Beheshti University of Medical Sciences, Tehran, Iran
[4]Department of Applied Cell Sciences, School of Advanced Technologies in Medicine, Tehran University of Medical Sciences, Tehran, Iran
[5]Department of Pathology, Faculty of Medicine, Urmia University of Medical Sciences, Urmia, Iran
[6]Department of Biostatistics, School of Allied Medical Sciences, Shahid Beheshti University of Medical Sciences, Tehran, Iran
[7]Science for Life Laboratory, Department of Medical Biochemistry and Biophysics, Karolinska Institute, Solna, Sweden

Received: June 2026**, Accepted:** July 2026

ABSTRACT

Background and Objectives: Influenza A virus remains a major global health concern because antigenic drift reduces the long-term efficacy of current vaccines. This study evaluated a multi-epitope DNA vaccine targeting conserved regions of hemagglutinin (HA) and polymerase acidic (PA) proteins from influenza A/H1N1 and A/H3N2 viruses.

Materials and Methods: Conserved B-cell, $CD4^+$ T-cell, and $CD8^+$ T-cell epitopes were identified using immunoinformatic tools and linked to β-defensin-2 in the pcDNA3.1(+) vector. Protein expression was confirmed in HEK293 cells. BALB/c mice were immunized intramuscularly and challenged with lethal doses of H1N1 or H3N2 viruses. Humoral and cellular immune responses, lung viral loads, histopathology, and clinical outcomes were assessed.

Results: Vaccinated mice exhibited undetectable or markedly reduced lung viral loads (1,000-10,000-fold; $p<0.01$), significantly decreased pulmonary lesions, and milder clinical manifestations than controls. Vaccination induced significant $CD4^+$ ($p=0.041$) and $CD8^+$ ($p=0.038$) T-cell responses in bronchoalveolar lavage fluid, accompanied by increased interferon-γ and interleukin-4 production, indicating balanced cellular and humoral immunity. Complete protection against mortality was observed following viral challenge.

Conclusion: This multi-epitope DNA vaccine elicited cross-protective immunity against influenza A/H1N1 and A/H3N2 by targeting conserved HA and PA epitopes, supporting its potential as a candidate for universal influenza vaccine development.

Keywords: Influenza A virus; H1N1 subtype; H3N2 subtype; Hemagglutinin; DNA vaccine

*Corresponding authors: Farhad Rezaei, Ph.D, Department of Virology, School of Public Health, Tehran University of Medical Sciences, Tehran, Iran. Tel: +98-9122161067 Fax: +98-88952343 Email: rezaie.farhad@gmail.com

Talat Mokhtari Azad, Ph.D, Department of Virology, School of Public Health, Tehran University of Medical Sciences, Tehran, Iran. Tel: +98-9121402396 Fax: +98-2188952343 Email: mokhtari@sina.tums.ac.ir

Copyright © 2026 The Authors. Published by Tehran University of Medical Sciences.
This work is licensed under a Creative Commons Attribution-Non Commercial 4.0 International license (https://creativecommons.org/licenses/by-nc/4.0/). Noncommercial uses of the work are permitted, provided the original work is properly cited.

INTRODUCTION

Influenza is a highly contagious respiratory infection that causes substantial global morbidity and mortality each year. Seasonal influenza leads to an estimated 290,000–650,000 deaths annually worldwide, according to World Health Organization (WHO) estimates (1). Influenza A viruses, particularly the H1N1 and H3N2 subtypes, evolve rapidly through antigenic drift, generating new variants that frequently reduce the effectiveness of strain-matched seasonal vaccines (2, 3). Current vaccines, which primarily target the hemagglutinin (HA) and neuraminidase (NA) surface proteins, must be reformulated annually and often provide suboptimal protection when circulating strains drift (4).

These limitations highlight the critical need for a universal influenza vaccine capable of inducing broad and durable immunity. Next-generation strategies increasingly focus on conserved viral regions—such as the HA stem and internal proteins like NP and PA to overcome antigenic variability (5). Advances in structural vaccinology, epitope engineering, and immunoinformatics have accelerated the design of multi-epitope vaccines that stimulate both humoral and cellular immunity (6, 7). DNA vaccines are of growing interest because they can simultaneously elicit B-cell responses and $CD4^+$/$CD8^+$ T-cell immunity (8). Modern computational tools enable precise prediction of immunodominant epitopes, and several multi-epitope influenza vaccine candidates have shown promising protective activity in preclinical and clinical studies (9).

In this study, a multi-epitope DNA vaccine incorporating conserved epitopes derived from the hemagglutinin (HA) and polymerase acidic (PA) proteins of influenza A virus was designed. By targeting antigenically conserved regions that are less susceptible to antigenic drift, broad cross-protective immunity against both H1N1 and H3N2 subtypes was hypothesized to be achieved. The immunogenicity and protective efficacy of the vaccine were evaluated in a BALB/c mouse model, and robust humoral and cellular immune responses, together with significant protection following viral challenge, were demonstrated. These findings suggest that conserved multi-epitope DNA vaccines represent a promising platform for the development of broadly protective influenza vaccines. Furthermore, the incorporation of additional highly conserved influenza antigens may further enhance the breadth and durability of protection, thereby contributing to the long-term goal of developing a universal influenza vaccine.

MATERIALS AND METHODS

In-silico design of the vaccine. A total of 540,000 influenza hemagglutinin (HA) sequences (H1 and H3 subtypes) and 24,000 polymerases acidic (PA) protein sequences were retrieved from the GISAID influenza virus database (https://gisaid.org/), representing a wide range of geographical regions. Following quality control steps, including trimming and redundancy filtering, 12,200 unique H1 sequences, 12,200 H3 sequences, and 1,200 PA sequences were obtained. Multiple sequence alignments were performed using the MAFFT online server version 7 and visualized with Jalview (CLUSTALW algorithm). Conserved regions with high sequence identity were selected for epitope prediction.

Cytotoxic T lymphocyte (CTL), helper T lymphocyte (HTL), and linear B-cell epitopes were predicted from the PA protein using a two-stage screening approach. Initial CTL epitope candidates, restricted to MHC class I alleles H-2-Dd, H-2-Ld, and H-2-Kd, were identified via the NetCTL 1.2 server. These were then filtered based on criteria including antigenicity, allergenicity, toxicity, and immunogenicity. High-affinity epitopes were further validated through molecular docking analysis.

HTL epitopes relevant to murine MHC class II alleles were predicted using the IEDB server and subjected to similar filtration criteria. For the B-cell epitope prediction of H1 and H3 HA proteins, four algorithms were employed to identify regions with high antigenicity and overlapping epitope potential. The predicted B-cell epitopes were further evaluated using IEDB tools for β-turn propensity, surface accessibility, flexibility, and immune-stimulatory potential (Figs. 1 and 2).

Cloning and expression of the construct, in vitro. The integrity of the pcDNA3.1 (+) plasmid was verified by PCR using the forward primer 5’-CGCAAATGGGCGGTAGGCGTG-3’ and reverse primer 5’-TAGAAGGCACAGTCGAGG-3’ with the QIAGEN Multiplex PCR kit, and the product was confirmed by Sanger sequencing. The recombinant PcDNA3.1 (+) plasmid was transformed into TOP10

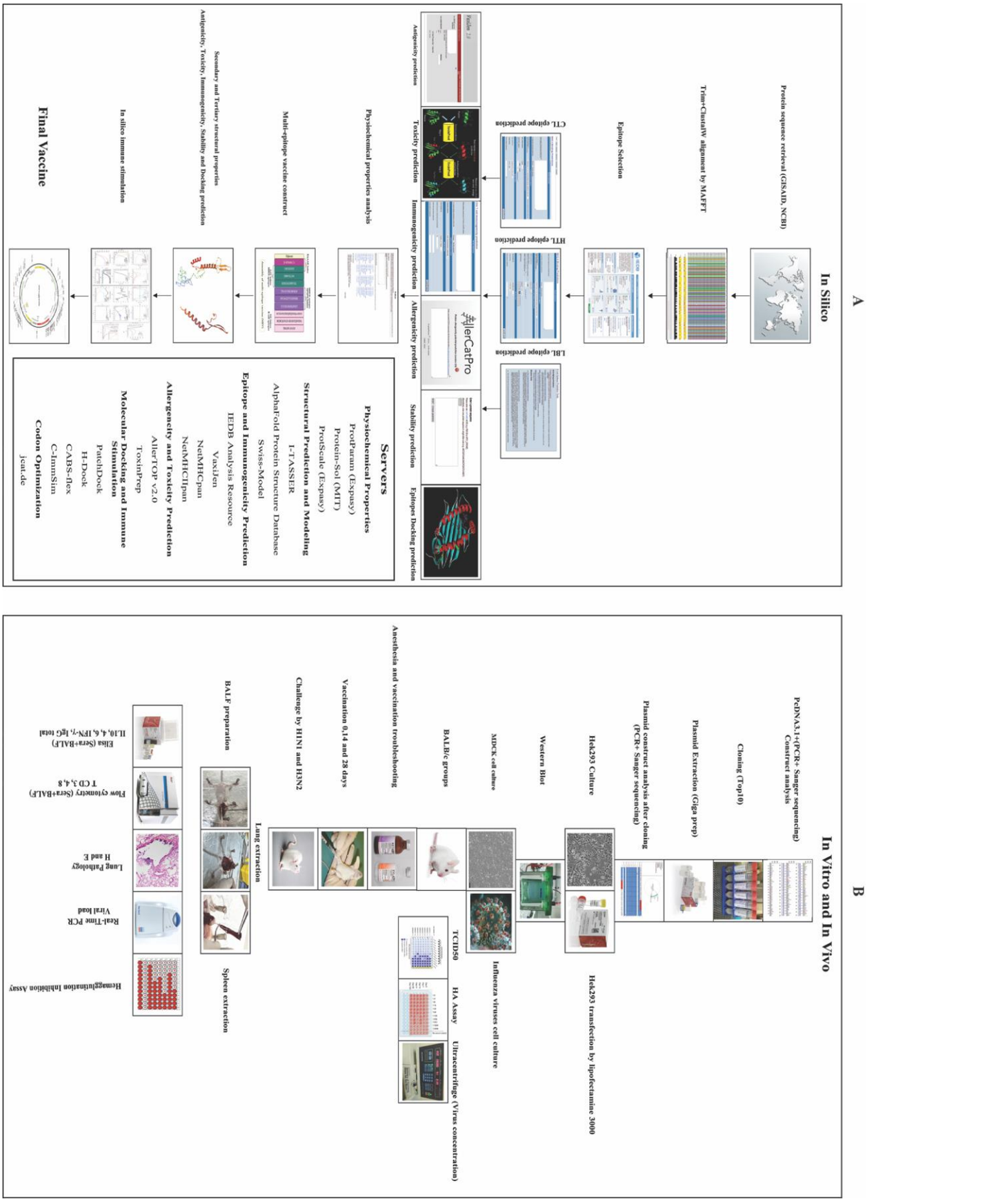


Fig. 1. (A) Schematic workflow for the in silico immunoinformatic processes (B) Schematic workflow for the in vitro and in vivo processes.

Fig. 2. B-cell epitope selection procedure by IEDB tools. In the first row of images, we identified the best regions with 99.99% repetition, from which the epitope was selected. Then, the selected epitopes were checked and verified using Bepipred Linear Epitope Prediction 2.0, Emini Surface Accessibility Prediction, Karplus & Schulz Flexibility Prediction, Kolaskar & Tongaonkar Antigenicity, and Parker Hydrophilicity Prediction.

E. coli cells (Invitrogen) and subsequently transfected into HEK293 cells. A GFP-expressing plasmid was used in parallel as a positive transfection control (10).

Cells were lysed using RIPA buffer (Thermo Fisher, USA). The cell pellet was resuspended in RIPA buffer and sonicated on ice. After 30 minutes of centrifugation at 12,000 g, 4°C, the supernatant was collected, aliquoted, and stored at -80°C until further processing. For western blotting, 20 µl of diluted protein lysates were loaded onto a 12% SDS-PAGE gel, electrophoresed, and transferred to a PVDF membrane (Roche). The membrane was blocked with BSA and incubated overnight at 4°C with a mouse anti-His monoclonal primary antibody (1:15,000, Invitrogen, USA) followed by an HRP-conjugated goat anti-mouse IgG secondary antibody (1: 3,000, Southern Biotech, Birmingham, AL) for 1 hour at room temperature. Reactive bands were visualized using the Pierce™ Fast Western Blot Kit and analyzed with an automated ECL analyzer (Fig. 1).

Influenza virus propagation and titration. Madin-Darby Canine Kidney (MDCK) cells were cultured in Dulbecco's Modified Eagle Medium (DMEM; Gibco, USA) supplemented with 5% fetal bovine serum (FBS; Gibco, USA) and 1% penicillin/streptomycin (Gibco, USA) at 37°C with 5% CO_2 for propagation and titration of the Influenza virus. Two mouse-adapted influenza A strains, A/Puerto Rico/8/1934(H1N1 (PR8)) and A/X31-H3N2, were obtained from the WHO and the National Institute for Medical Research (NIMR), London. For titration, MDCK cells at 85% confluency in U-bottom 96-well plates were washed with phosphate-buffered saline (PBS), inoculated with 100 µL of 10-fold serial dilutions of each virus strain in serum-free DMEM containing 1 µg/mL TPCK-trypsin, and incubated at 37°C for 60 h. The 50% tissue culture infectious dose ($TCID_{50}$) was calculated using the Reed-Muench method. For hemagglutination assays, viruses were serially diluted 2-fold in PBS, mixed with chicken RBCs (for H3N2) or human RBCs (for H1N1), and incubated at 4°C for 30 min; hemagglutination units (HAU/mL) were determined from RBC sedimentation.

Animal experiments. Six to eight-week-old female BALB/c mice were obtained from the Laboratory Animal Center of the Pharmacology Center of Iran and housed at 25°C with a 12-hour light/dark cycle. All experiments were approved by the Research and Ethics Committee of the Tehran University of Medical Sciences (IR.TUMS.SPH.REC.1399.185). This research was executed and documented by the ARRIVE (Animal Research: Reporting of in Vivo Experiments) guidelines, promoting transparency and reproducibility in animal studies, and all methods were carried out by relevant guidelines and regulations. In the designation of the treatment groups, the BALB/c mice were divided into six groups of eight. The plasmid dosage for injections was determined using spectrophotometry and set to be 50 µg per injection. Mice in the first and third groups received 50 µL of a multi-epitope vaccine on days 0, 14, and 28, followed by a challenge with 30 µL of PBS containing 5 × LD_{50} of H1N1 and H3N2, respectively, four weeks after the final immunization. The second and fourth groups served as controls, receiving PBS injections instead of the vaccine, and were challenged with H1N1 and H3N2, respectively. The fifth and sixth groups received normal saline and empty pcDNA3.1 (+), respectively, as additional controls without viral challenge. After the viral challenge, mice were weighed daily and monitored for clinical symptoms such as lethargy and ruffled fur on day nine post-infection. The mice were euthanized with ketamine (80-100 mg/kg) and xylazine (5-10 mg/kg) Intraperitoneal (IP) injection (11) before being sacrificed for bronchoalveolar lavage (BAL) and pathological analysis (Fig. 1).

Detection of IgG and inflammatory cytokines by ELISA method. A single-use lancet was used to draw blood from the submandibular region of mice, providing a humane, efficient, and cost-effective method for obtaining samples. Serum and bronchoalveolar lavage (BAL) levels of IFN-γ (Cat # 88-7314-22), IL-4 (Cat # 88-7044-22) , IL-10 (Cat # 88-7105-22), and IL-6 (Cat # 88-7044-22) were measured using Thermo Fisher ELISA kits, with positive results defined as OD values exceeding 2.0-fold the negative control (12).

To evaluate total IgG, a SPL 96-well ELISA plate was coated with 50 ng of influenza split-virus vaccine per well. Ten-fold serial dilutions of mice sera were added, incubated at room temperature overnight, and then washed with PBS. Afterward, HRP-conjugated anti-mouse IgG was added and incubated for 30 minutes. Following another wash, the secondary antibody (HRP-conjugated anti-mouse IgG), TMB substrate, stop solution (2N H_2SO_4), and sample volumes (100 µL) were added under plate coating conditions (over-

night at 4°C). The OD was measured at 450 nm using a Combiwash REF 18460 microplate reader.

Microneutralization assay for detection of neutralizing antibodies against H1N1 and H3N2. Neutralizing antibody responses against influenza A H1N1 and H3N2 viruses were evaluated using a standard microneutralization (MN) assay in MDCK cell culture, following WHO-recommended protocols with minor modifications. Briefly, sera were heat-inactivated at 56°C for 30 min to eliminate complement activity and then serially two-fold diluted in serum-free DMEM. Equal volumes of diluted sera were incubated with 100 $TCID_{50}$ of homologous H1N1 or H3N2 virus for 1 h at 37°C to allow antibody–virus neutralization. Following incubation, the serum–virus mixtures were added to confluent MDCK cell monolayers seeded in 96-well plates and maintained in infection medium containing DMEM supplemented with 1-2 µg/mL TPCK-treated trypsin. Plates were incubated at 37°C with 5% CO_2 for 72 h. Virus-only wells served as positive infection controls, while cell-only wells were included as negative controls. Neutralization was assessed by visual inspection of cytopathic effect (CPE) under an inverted microscope. The microneutralization titer was defined as the highest serum dilution that completely inhibited virus-induced CPE in at least 50% of replicate wells. In selected experiments, viral inhibition was further confirmed by ELISA-based detection of viral nucleoprotein (NP) in cell supernatants. MN titers were expressed as the reciprocal of the highest neutralizing serum dilution (13).

Flow cytometry (spleen and BAL). The flow cytometry was intended to evaluate activation of T-cell subsets ($CD3^+$, $CD4^+$, $CD8^+$) in the spleen and BAL. The cells were stained with fluorophore-conjugated antibodies in a solution containing 2% BSA and 1 mM EDTA in PBS and kept on ice for 30 minutes. Subsequently, the samples were analyzed using the BD FACS Calibur flow cytometer (BD Biosciences, San Jose, CA). The following antibodies were utilized: anti-mouse CD4 APC (Catalog No: 100412, BioLegend), anti-mouse CD8 PE (Catalog No: 100707, BioLegend), and anti-mouse CD3 PerCP-Cy5.5 (Catalog No: 100217, BioLegend). Data were processed with FlowJo software version 10 (TreeStar).

Quantitative RT-PCR for evaluation of viral load. Quantitative qRT-PCR (qPCR) was performed to assess the viral load differences between vaccinated mice and their unvaccinated controls. Mice's BAL using the QIAamp® Viral RNA mini kit (QIAGEN, Germany), and one-step qPCR was performed using the genesig® Standard Kit.

Histopathology experiments. Both left and right lungs were fixed in 10% natural buffered formalin and processed for hematoxylin and eosin (H&E) staining according to protocol (14). Each mouse lung contributed three tissue sections and was independently assessed by two researchers under a microscope at 200× magnification to assess morphological changes and identify any pathological features.

Statistical analysis. Normality of data distribution was first assessed using the Shapiro–Wilk test. When the assumption of normality was satisfied ($P > 0.05$), parametric comparisons between groups were performed using an unpaired two-tailed Student's t-test, with analyses conducted separately for BAL and serum samples. For datasets that did not meet normality assumptions, the non-parametric Mann–Whitney U test was applied. In addition to p-values, effect sizes were calculated to quantify the magnitude of observed differences. For parametric comparisons, Cohen's d was computed and interpreted according to conventional thresholds (0.2 = small, 0.5 = medium, 0.8 = large effect). For non-parametric analyses, effect sizes were estimated using rank-based measures where appropriate. Reporting effect sizes alongside significance testing was performed to enhance statistical transparency and biological interpretability. A two-sided significance level of 0.05 was applied for all analyses. Statistical analyses were conducted using Stata and GraphPad Prism (version 10.0), and data visualization was performed using Python 3.12.0 with the *matplotlib* package.

RESULTS

In-silico: sequences extraction procedure. The aligned and filtered sequences were subjected to IEDB to calculate all possible epitopes. As a result, 1400, 1600, and 1540 epitopes were obtained for B cells, MHCI, and MHCII, respectively. The IEDB tool was further utilized on B-cell epitopes for surface accessibility, flexibility prediction, antigenicity,

and hydrophobicity prediction. Finally, high-score epitopes were selected (Fig. 2). Molecular docking studies were conducted to evaluate the binding affinity and interaction patterns of the influenza DNA vaccine components with immune system receptors. The docking results indicated a strong binding affinity between the designed vaccine epitopes and MHC-I, FMYSDFHFI (binding energy: -223.42 kcal/mol), INPNYLLSW (binding energy: -161.29 kcal/mol), KPHEKGINPNYLL (binding energy: -210.68 kcal/mol) and MHC-II, TNLYGFIIKGRSHLR (binding energy: -210.68 kcal/mol), FFGWKEPYIVKPHEK (binding energy: -241.49 kcal/mol), YGFIIKGRSHLRNDT (binding energy: -215.09 kcal/mol) (Fig. 3). The C-IMMUNE server analysis predicted that the designed vaccine construct exhibits high immunogenic potential, with an overall immunogenicity score of 29.2 for B cell epitopes and 26.4 for MHC I and MHC II epitopes (Fig. 4).

The construct showed strong B-cell and T-cell epitope coverage, suggesting its potential for broad immune activation. The mentioned epitopes from the H1H3 and PA proteins consensus sequences of H1N1 and H3N2 were used to construct the vaccine. Adjuvant (beta-defensin-2), linkers, and 6-His-tags were also embedded in the final structure of the vaccine. Thus, the final vaccine structure comprised 223 amino acids. The antigenicity score of the assembled vaccine was 0.6819 when examined in the VaxiJen server. Also, the vaccine protein was non-allergenic in the AllerTOP server. The predicted vaccine weighed 24.6 kilodaltons and possessed a theoretical isoelectric point of 9.7, indicating the proposed vaccine had an alkaline pH. Negatively and positively charged residues were 14 and 31, respectively. The grand average water affinity was -0.711, suggesting a hydrophilic vaccine. The I-TASSER server functional annotation predicted potential binding to immune receptors, supporting its suitability for vaccine development (Fig. 5). Fig. 5 shows a summary of the immunoinformatics procedure and Ramachandran plot 97.92%, indicating our designated vaccine is structurally stable and suitable for wet-lab validation. The final sequence of the epitopes is presented in Table 1.

In vitro experiments. The pcDNA3.1 (+) (BHT) plasmid was used to transform *E. coli* TOP10 cells and subsequently amplified. The recombinant plasmid, pcDNA3.1 (+)/ (BHT), was then extracted using the PureLink™ HiPure Expi Plasmid Gigaprep Kit. The construct was verified by PCR, restriction enzyme digestion with *NdeI* and *XbaI*, and DNA sequencing. Transfections were carried out using three groups: pcDNA3.1 (BHT) containing the construct, pcDNA3.1 (GFP) as a vector without an insert, and HEK293 cells without any vector as a negative control. After 24 to 48 hours, cell lysates from the transfected and control groups were analyzed by Western blot for immunodetection. The analysis confirmed the expression of BTH sequences at the expected molecular weight of 24 kDa. The results validated the ability of the plasmid to express the designed multi-epitope construct, supporting its use in subsequent experimental procedures.

In vivo experiment: 1 evidence of vaccine protection through clinical observations. Signs of illness include ruffled fur, hunched posture, rapid breathing, inactivity, and paralysis of the posterior limb. In contrast, these clinical signs were delayed for 2–3 days in mice immunized with PcDNA3.1 (+)/BTH, in which they also exhibited mild clinical signs and slight weight loss, and then began to recover (Figs. 6 A-E).

Real-time PCR. Following the challenge, all mice exhibited clear symptoms of viral infection. To evaluate changes in lung viral load after immunization, BALF samples were collected nine days post-challenge for viral quantification. The lung viral titers in vaccinated mice were significantly lower than those in the non-vaccinated control groups (Fig. 6F).

IL-10 (BAL and sera). BAL and serum IL-10 levels showed no significant difference between vaccinated and challenged control groups for either H1N1 (VH1 vs. CH1; $P = 0.3098$) or H3N2 (VH3 vs. CH3; $P = 0.0577$), with small-to-medium effect sizes (Cohen's $d \approx 0.3–0.5$). However, both VH1 and VH3 were significantly higher than non-intervention controls (NS and EP) (VH1: $P = 0.0163$ vs NS, $P = 0.0247$ vs EP; VH3: $P = 0.0056$ vs NS, $P = 0.0021$ vs EP), with very large effect sizes (Cohen's $d > 2$), reflecting strong local anti-inflammatory responses. In sera, a similar pattern was observed: VH1 and VH3 were not significantly different from their respective challenged controls (VH1 vs CH1: $P = 0.2033$; VH3 vs CH3: $P = 0.0829$; Cohen's $d \approx 0.5–0.6$) but were markedly elevated compared to NS and EP ($P < 0.0001$; Cohen's

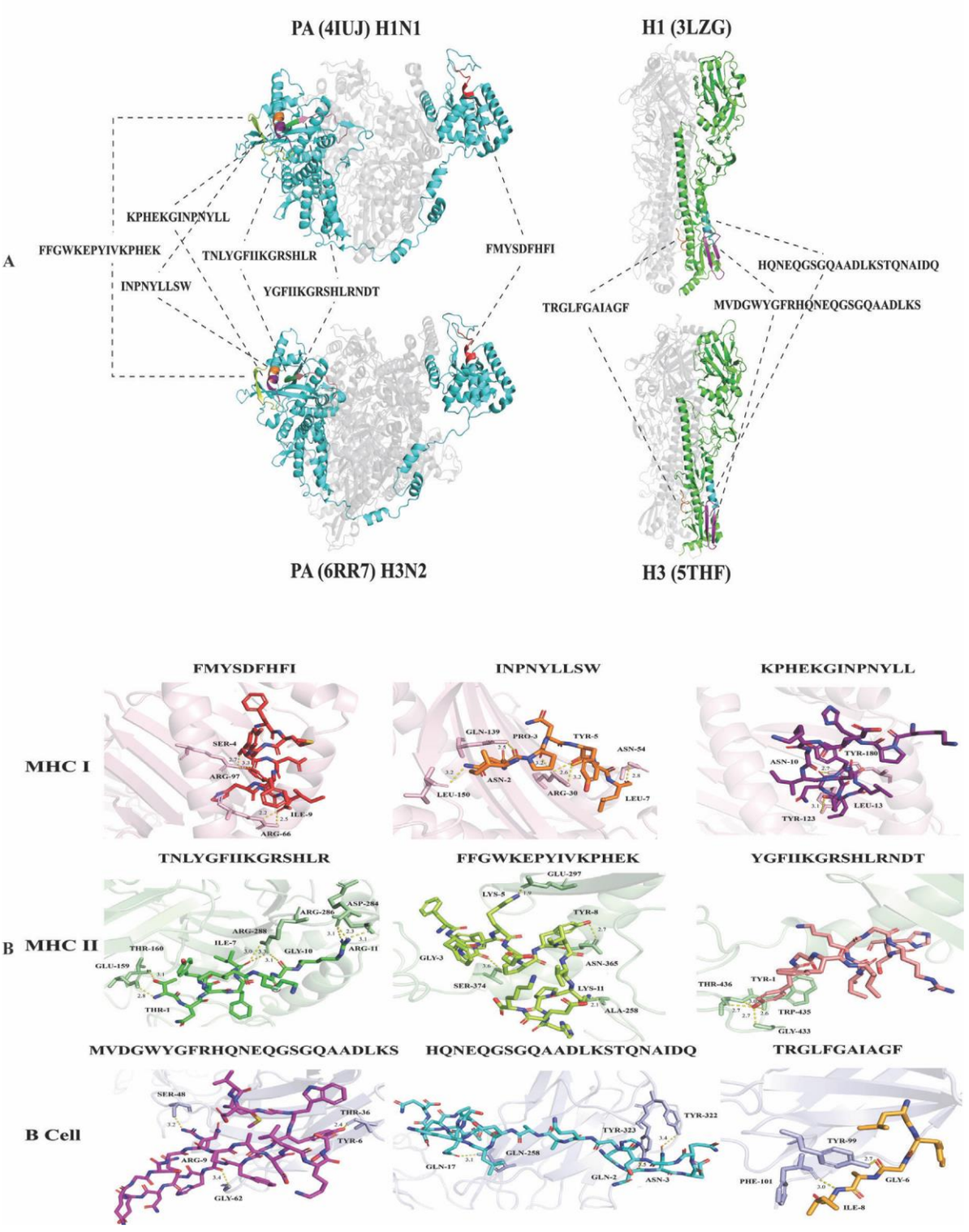
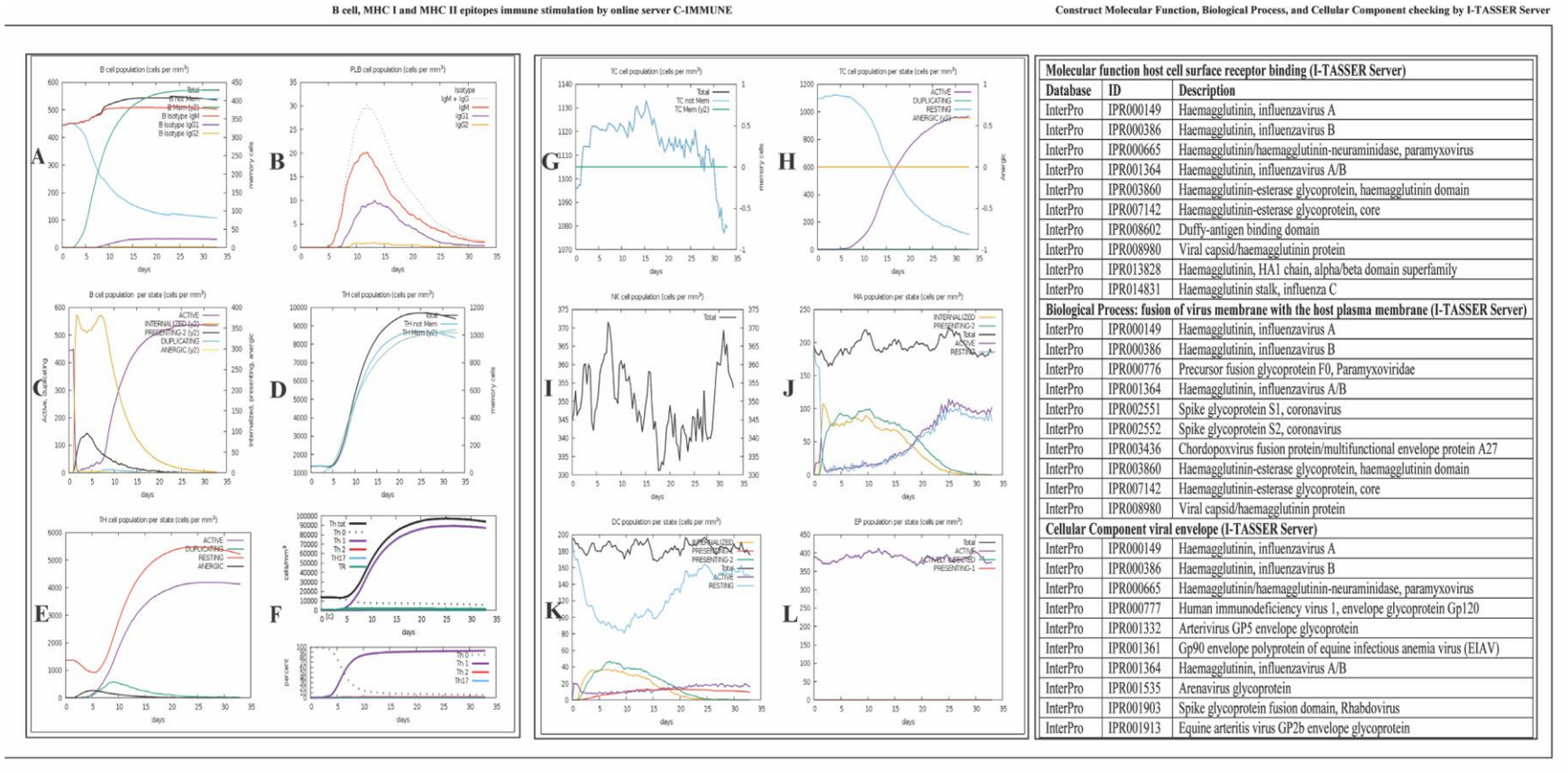


Fig. 3. (A) Selected epitope positions in PA, H1, and H3 proteins 3D structure (B) PA Epitope docking for MHC I (H-2-Dd, H-2-Ld, and H-2-Kd), MHC II (H2-IAd and H2-IEd), and B cell epitopes for Mouse IgG Fab (PDB: 1AE6).



Molecular function host cell surface receptor binding (I-TASSER Server)		
Database	**ID**	**Description**
InterPro	IPR000149	Haemagglutinin, influenzavirus A
InterPro	IPR000386	Haemagglutinin, influenzavirus B
InterPro	IPR000665	Haemagglutinin/haemagglutinin-neuraminidase, paramyxovirus
InterPro	IPR001364	Haemagglutinin, influenzavirus A/B
InterPro	IPR003860	Haemagglutinin-esterase glycoprotein, haemagglutinin domain
InterPro	IPR007142	Haemagglutinin-esterase glycoprotein, core
InterPro	IPR008602	Duffy-antigen binding domain
InterPro	IPR008980	Viral capsid/haemagglutinin protein
InterPro	IPR013828	Haemagglutinin, HA1 chain, alpha/beta domain superfamily
InterPro	IPR014831	Haemagglutinin stalk, influenza C
Biological Process: fusion of virus membrane with the host plasma membrane (I-TASSER Server)		
InterPro	IPR000149	Haemagglutinin, influenzavirus A
InterPro	IPR000386	Haemagglutinin, influenzavirus B
InterPro	IPR000776	Precursor fusion glycoprotein F0, Paramyxoviridae
InterPro	IPR001364	Haemagglutinin, influenzavirus A/B
InterPro	IPR002551	Spike glycoprotein S1, coronavirus
InterPro	IPR002552	Spike glycoprotein S2, coronavirus
InterPro	IPR003436	Chordopoxvirus fusion protein/multifunctional envelope protein A27
InterPro	IPR003860	Haemagglutinin-esterase glycoprotein, haemagglutinin domain
InterPro	IPR007142	Haemagglutinin-esterase glycoprotein, core
InterPro	IPR008980	Viral capsid/haemagglutinin protein
Cellular Component viral envelope (I-TASSER Server)		
InterPro	IPR000149	Haemagglutinin, influenzavirus A
InterPro	IPR000386	Haemagglutinin, influenzavirus B
InterPro	IPR000665	Haemagglutinin/haemagglutinin-neuraminidase, paramyxovirus
InterPro	IPR000777	Human immunodeficiency virus 1, envelope glycoprotein Gp120
InterPro	IPR001332	Arterivirus GP5 envelope glycoprotein
InterPro	IPR001361	Gp90 envelope polyprotein of equine infectious anemia virus (EIAV)
InterPro	IPR001364	Haemagglutinin, influenzavirus A/B
InterPro	IPR001535	Arenavirus glycoprotein
InterPro	IPR001903	Spike glycoprotein fusion domain, Rhabdovirus
InterPro	IPR001913	Equine arteritis virus GP2b envelope glycoprotein

Fig. 4. Immune stimulation analysis of B cell, MHC I, and MHC II epitopes using the C-IMMSIM online server, simulating three doses of the multi-epitope DNA vaccine. (A) The B cell population (cells/mm³) showed a marked increase following immunization. (B) The plasma B cell (PLB) population demonstrated elevated levels of IgM and IgG. (C) The distribution of B cells by activation state revealed a high proportion of active B cells. (D) The total helper T (TH) cell population increased significantly. (E) The TH cell population by activation state also showed a high level of active cells. (F) The Th1 and total TH cell graphs indicated robust helper T cell responses. (G) Cytotoxic T cell (TC) population peaked during the vaccination period. (H) TC cell population by state confirmed a high level of active cytotoxic cells. (I) The natural killer (NK) cell population increased over time. (J) The Macrophage (MA) population by state showed a rise, particularly after 35 days. (K) The dendritic cell (DC) population by state demonstrated enhanced antigen-presenting cell activation. (L) The eosinophil (EP) population by state also increased post-vaccination. The accompanying table presents results from the I-TASSER server, indicating the vaccine construct's molecular function, biological processes, and cellular component predictions. These findings confirm that the designed multi-epitope vaccine preserves critical structural and functional attributes of influenza viral proteins, supporting its potential to elicit a strong and specific immune response. "Per state" refers to the functional or activation state of immune cells in the immune simulation (naïve, active, or memory).

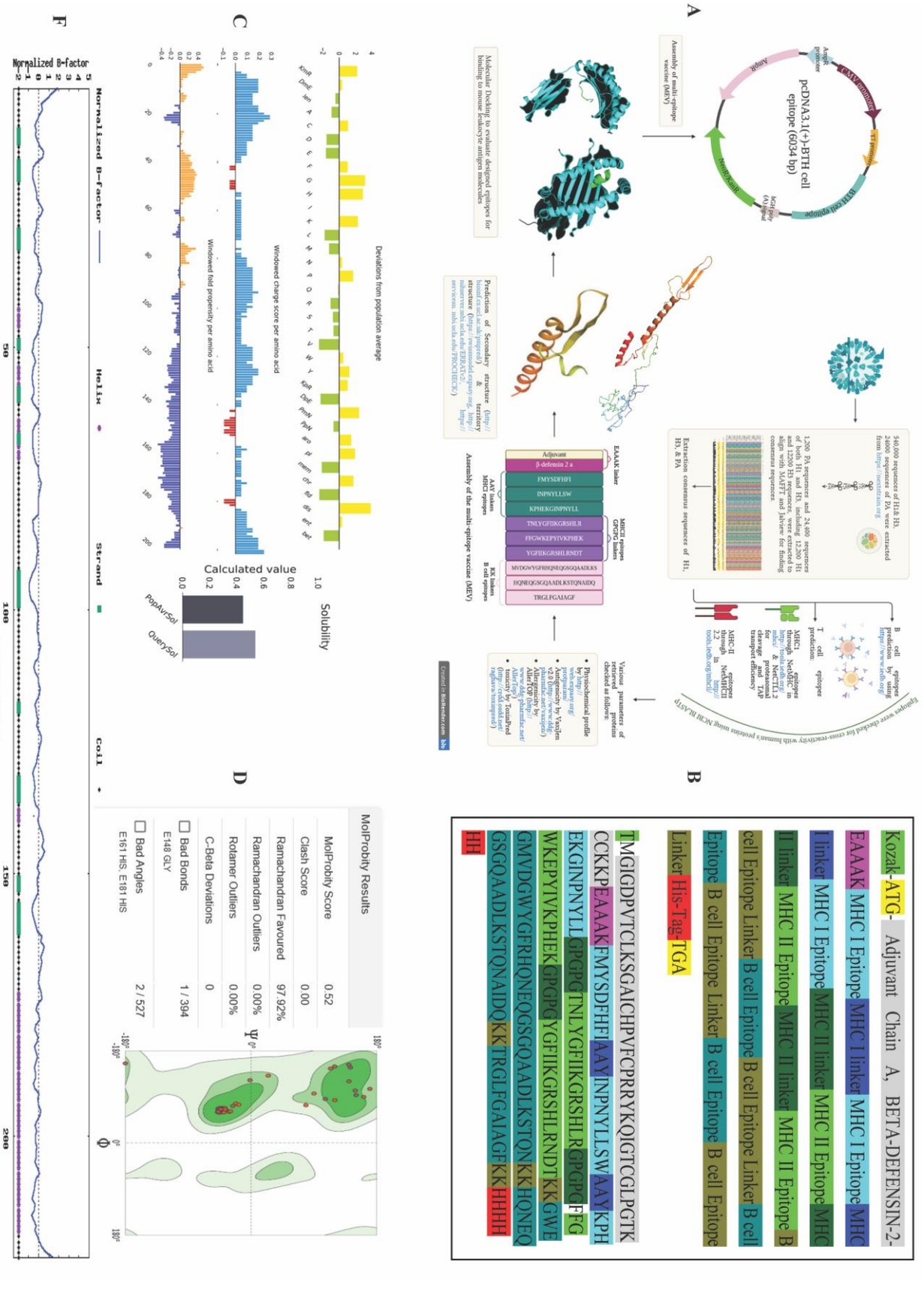


Fig. 5. (A) Schematic representation of the in silico immunoinformatics workflow used to design a multi-epitope vaccine candidate against Influenza A (H1N1 and H3N2) viruses. (B) The final plasmid construct includes the following elements in sequence: a 5′ HindIII restriction site, Kozak sequence (green), start codon ATG (Yellow), adjuvant chain A (Gray) composed of beta-defensin-2 and EAAAK linker, followed by three MHC I epitopes (Light blue) separated by MHC I linkers, three MHC II epitopes (light green) separated by MHC II linkers, and three B cell epitopes (Dark blue) separated by B cell-specific linkers. The construct ends with a His-tag, stop codon (TGA, Red), and a 3′ XbaI restriction site. (C) Vaccine solubility prediction compared to *E. coli* protein solubility, analyzed using the Protein-sol server. (D) Ramachandran plot analysis showing that 97.92% of residues fall within the most favored regions, indicating a high-quality structural model. (E) Tertiary structure stability prediction performed using the I-TASSER server.

Table 1. B cell, MHC I, and MHC II epitope sequences.

B cell epitopes	Antigenicity	Toxicity	Immunogenicity	Allergenicity	Stability	Docking
MVDGWYGFRHQNEQGSGQAADLKS	Yes	No	Yes	No	Yes	Yes
HQNEQGSGQAADLKSTQNAIDQ	Yes	No	Yes	No	Yes	Yes
TRGLFGAIAGF	Yes	No	Yes	No	Yes	Yes

MHC I epitopes	Allele	Antigenicity	Toxicity	Immunogenicity	Allergenicity	Stability	Docking
FMYSDFHFI	H-2-Kd	Yes	No	default	No	Yes	-223.42
INPNYLLSW	H-2-Dd	Yes	No	custom	No	Yes	-161.29
KPHEKGINPNYLL	H-2-Ld	Yes	No	custom	No	Yes	-195.67

MHC II epitopes	Allele	Antigenicity	Toxicity	Immunogenicity	Allergenicity	Stability	Docking
TNLYGFIIKGRSHLR	H2-IEd	Yes	No	custom	No	Yes	-210.68
FFGWKEPYIVKPHEK	H2-IAd	Yes	No	custom	No	Yes	-241.49
YGFIIKGRSHLRNDT	H2-IEd	Yes	No	custom	No	Yes	-215.09

Cytotoxic T lymphocytes (CTL) epitope prediction by (NetMHCpan), helper T lymphocytes (HTL) epitope prediction by (NetMHCIIpan), and linear B-cell (LBL) epitope prediction by (IEDB tools). Antigenicity, toxicity, immunogenicity, allergenicity, predicted epitope stability, and Codon Optimization were assessed using AllerTOP v2.0, ToxinPrep, Expasy tools, and jcat.de. Molecular docking was performed using the HDock and PatchDock programs. Physicochemical properties were analyzed with ProtParam (Expasy), Protein-Sol (MIT), and ProtScale (Expasy). All epitopes pass antigenicity, toxicity, immunogenicity, stability, and docking analysis tests.

d > 2). These results indicate that the multi-epitope DNA vaccine effectively enhances IL-10-mediated immunoregulatory responses while maintaining comparable levels to challenged controls, highlighting its potential to modulate both local and systemic anti-inflammatory pathways (Fig. 7A).

IFN-γ (BAL and sera). IFN-γ levels in BAL fluid were markedly increased in both VH1 and VH3 vaccinated groups compared with their respective challenged control groups (CH1 and CH3), with highly significant differences ($P < 0.0001$). Effect size analysis revealed very large to extremely large effects for these comparisons (Cohen's $d = 4.71$ for VH1 vs. CH1 and $d = 3.21$ for VH3 vs. CH3), indicating a strong biological impact of vaccination on local Th1-type immune responses. IFN-γ expression in vaccinated groups was also substantially higher than in the non-intervention groups receiving normal saline (NS) or empty plasmid (EP) ($P < 0.0001$), with extremely large effect sizes ($d > 7.8$), confirming robust vaccine-induced activation of pulmonary cellular immunity. A similar pattern was observed in serum samples. Both VH1 and VH3 groups displayed significantly elevated IFN-γ levels compared with CH1 ($P < 0.001$) and CH3 ($P < 0.001$ and $P < 0.0001$, respectively). Effect size analysis further supported these findings, demonstrating large to very large effects for vaccinated versus challenged control in comparisons (Cohen's d > 3), and very large effects relative to NS and EP groups ($d > 0.8$). Together, these results indicate that the multi-epitope DNA vaccine induces a potent and biologically meaningful Th1-skewed immune response at both local (BAL) and systemic (serum) levels (Fig. 7B).

IL-6 (sera). Serum IL-6 levels were significantly higher in challenged control groups (CH1 and CH3) compared to vaccinated groups (VH1 and VH3), indicating pronounced inflammation in the absence of vaccination (VH1: 195.7 ± 33.5 pg/ml vs CH1: 270.4 ± 57.2 pg/ml; VH3: 174.8 ± 8.6 pg/ml vs CH3: 367.0 ± 67.2 pg/ml). These differences were associated with large to very large effect sizes (VH1 vs CH1: Cohen's $d \approx 1.4$; VH3 vs CH3: $d \approx 2.0–2.2$), underscoring the substantial magnitude of IL-6 modulation by vaccination. Furthermore, vaccinated groups exhibited significantly higher IL-6 levels than the non-intervention groups (NS and EP), reflecting an active immune response following challenge ($P < 0.0001$), with moderate-to-large effect sizes relative to EP ($d \approx 0.8–1.0$) and a large effect size relative to NS ($d \approx 1.5$). Collectively, these findings indicate that vaccination effectively mitigates excessive IL-6–mediated inflammation while preserving immune activation, highlighting its role in regulating inflammatory re-

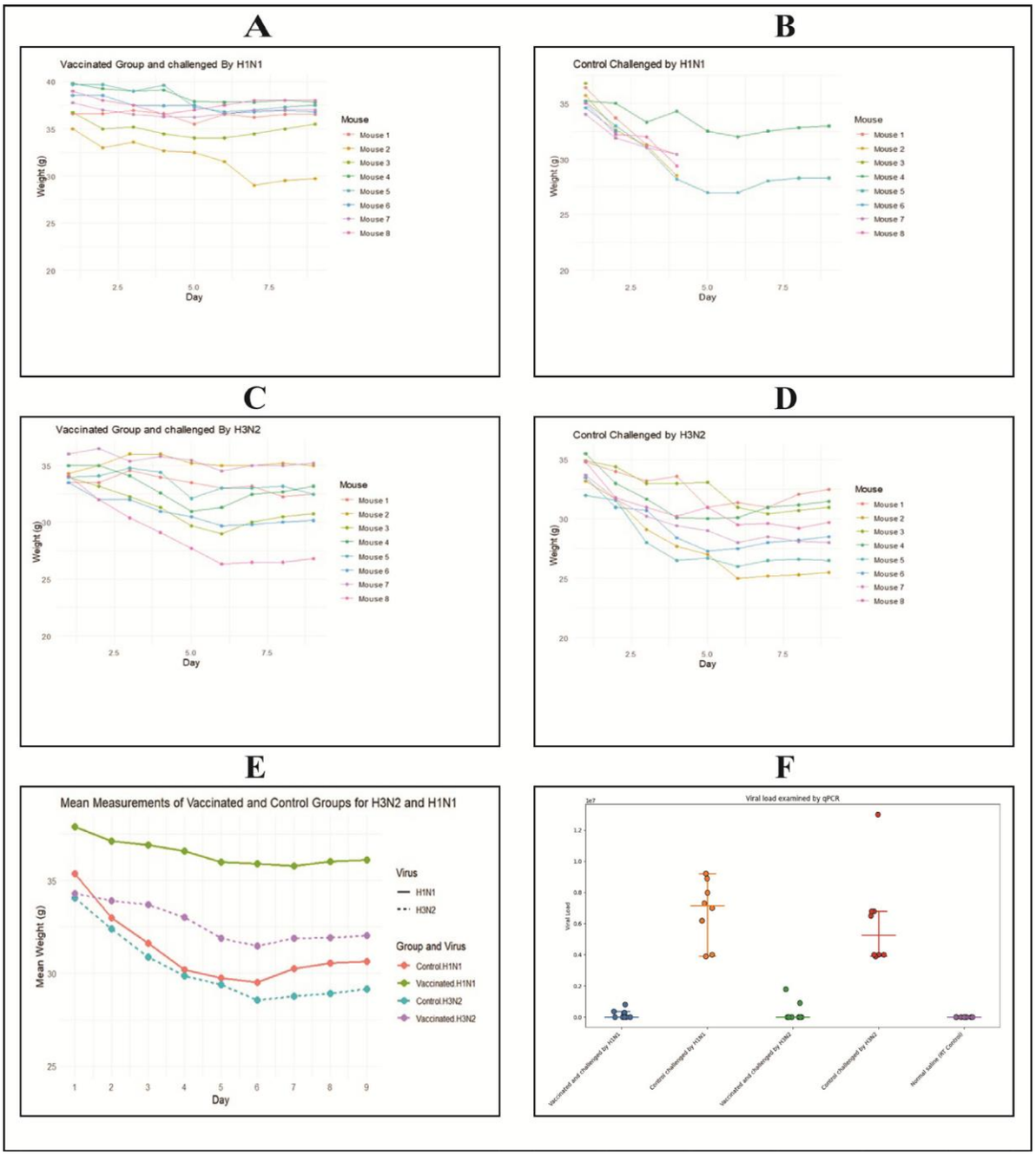


Fig. 6. Body weight changes and viral load in BALB/c mice across different experimental groups. (A) Weight change in the vaccinated group challenged with H1N1. (B) Weight change in the control group challenged with H1N1. (C) Weight change in the vaccinated group challenged with H3N2. (D) Weight change in the control group challenged with H3N2. (E) Comparison of mean weight measurements between vaccinated and control groups for both H1N1 and H3N2, showing statistically significant differences ($P < 0.05$). (F) Comparison of viral load between vaccinated and control groups. The Mann-Whitney U test revealed significant reductions in viral load in the vaccinated groups: for H1N1, $P = 0.0008$; and for H3N2, $P = 0.0126$, indicating the vaccine's strong efficacy in reducing viral replication. VH1: Vaccinated group, challenged with H1N1, CH1: Control group, challenged with H1N1, VH3: Vaccinated group, challenged with H3N2, CH3: Control group, challenged with H3N2, EP: Control group injected with empty plasmid, NS: Control group injected with normal saline. (8 mice per group)

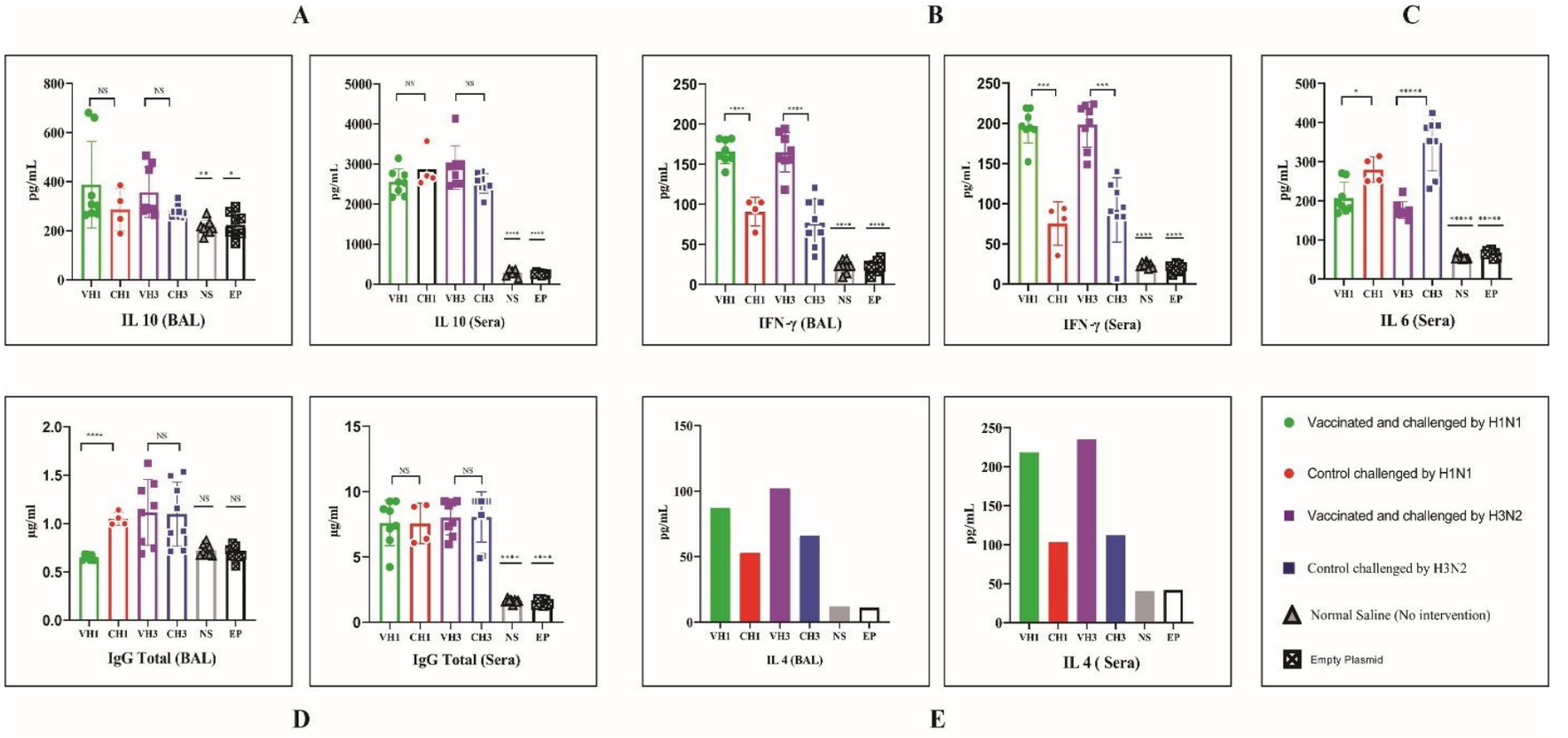


Fig. 7. T-test and Cohen's d analyses: (A) No significant difference in IL-10 levels was observed between vaccinated and control groups in both BAL and sera. (B) IFN-γ levels were significantly higher in the vaccinated groups compared to the control groups in both H1N1 and H3N2 challenge models (P = 0.0001). (C) Hemagglutination inhibition (HI) titers in BAL and sera were significantly elevated in vaccinated groups compared to control, normal saline, and empty plasmid-injected groups (P = 0.0001). (D) IL-6 levels in sera were higher in the challenged control groups than in the vaccinated groups (VH1 < CH1, P = 0.0114; VH3 < CH3, P < 0.0001). (E) Total IgG levels in BAL and sera were also higher in the control groups. (F) IL-4 levels in BAL and sera were significantly elevated in the vaccinated groups compared to the control groups. (*P < 0.05, **P < 0.01, ***P < 0.001, ****P < 0.0001). VH1: Vaccinated group, challenged with H1N1, CH1: Control group, challenged with H1N1, VH3: Vaccinated group, challenged with H3N2, CH3: Control group, challenged with H3N2, EP: Control group injected with empty plasmid, NS: Control group injected with normal saline. (8 mice per group).

sponses post-challenge (15) (Fig. 7D).

Influenza-specific IgG response analysis in immunized mice (BAL and sera). In BAL, total IgG levels were significantly lower in the vaccinated H1N1 group (VH1) compared to the H1N1-challenged control group (CH1) ($P < 0.0001$; Cohen's $d \approx 0.4$), indicating a less pronounced humoral response in the lungs. No significant difference was observed between the vaccinated H3N2 group (VH3) and its control (CH3) ($P = 0.9240$; Cohen's $d \approx 0.15$). Compared to non-intervention groups, both VH1 and VH3 exhibited markedly elevated IgG levels versus NS and EP (VH1: $P = 0.0001$; VH3: $P < 0.0001$), with very large effect sizes (Cohen's $d > 2$), demonstrating effective antibody induction by vaccination. In serum, total IgG levels were significantly higher in both VH1 and VH3 compared to their respective controls (CH1 and CH3) (VH1: $P < 0.001$; VH3: $P < 0.001$), as well as versus NS and EP ($P < 0.0001$ for both), with medium effect sizes observed for vaccinated versus challenged controls (Cohen's $d \approx 0.4–0.6$). These findings confirm that the DNA vaccine successfully stimulated systemic IgG responses, particularly evident in sera, highlighting robust immunogenicity against both H1N1 and H3N2 strains (Fig. 7E).

IL-4 (BAL and sera). IL-4 levels in vaccinated groups, in both BAL and sera, were significantly higher than in control, NS, and EP groups. In BAL, VH1 showed 87.1 pg/ml versus 53 pg/ml in CH1, and VH3 exhibited 102 pg/ml versus 66 pg/ml in CH3, indicating enhanced Th2 responses. Effect sizes for vaccinated versus challenged controls were medium (Cohen's $d \approx 0.5$), while comparisons with NS (12 pg/ml) and EP (11 pg/ml) showed very large effects (Cohen's $d > 2$). In sera, VH1 and VH3 showed 218.3 pg/ml and 235 pg/ml, respectively, versus 103 pg/ml (CH1) and 112 pg/ml (CH3), with medium-to-large effect sizes (Cohen's $d \approx 0.6–0.8$) and very large effects compared to NS (40.56 pg/ml) and EP (42 pg/ml) (Cohen's $d > 2$). These results indicate that the vaccine effectively stimulated Th2-mediated immunity, particularly systemically, enhancing helper T cell responses against both H1N1 and H3N2 strains (Fig. 7F).

Microneutralization antibody responses against H1N1 and H3N2. Microneutralization (MN) assays were performed in MDCK cell cultures to evaluate functional neutralizing antibody responses against H1N1 and H3N2 influenza viruses. Neutralizing titers were expressed as the reciprocal of the highest serum dilution that completely inhibited virus-induced cytopathic effect. For H1N1, vaccinated mice exhibited significantly higher MN titers compared to challenged control animals (VH1 vs. CH1; $P < 0.001$). Effect size analysis demonstrated a large to very large effect (Cohen's $d \approx 1.2–1.8$), indicating a robust biologically meaningful enhancement of neutralizing activity following vaccination. MN titers in the VH1 group were also markedly higher than those observed in the normal saline (NS) and empty plasmid (EP) groups ($P < 0.0001$), with very large effect sizes (Cohen's $d > 2$), whereas differences between NS and EP groups were negligible. Similarly, for H3N2, the vaccinated group (VH3) showed significantly elevated MN titers compared to the challenged control group (CH3; $P < 0.001$). The corresponding effect size was very large (Cohen's $d \approx 1.5–2.0$), confirming strong vaccine-induced neutralizing antibody responses. Comparisons between VH3 and non-intervention controls (NS and EP) also yielded extremely large effect sizes (Cohen's $d > 2$), while NS and EP groups did not differ meaningfully.

Flow cytometry and histopathological analysis revealed vaccine's strong protective impact. Flow cytometry and histopathological analysis of lung tissues from H1N1- and H3N2-infected mice revealed significant immunological differences between vaccinated and non-vaccinated groups. Vaccinated mice exhibited higher frequencies of $CD3^+$ and $CD4^+$ T cells in both BAL fluid and spleen, with statistically significant increases observed in the H1N1 group ($CD3^+$: $p = 0.0229$; $CD4^+$: $P = 0.0181$) and the H3N2 group ($CD3^+$: $P = 0.0390$; $CD4^+$: $P = 0.0031$). Although $CD8^+$ T cells were mildly elevated depending on lung lesion in vaccinated mice compared to the normal saline group (H1N1: $P = 0.0045$; H3N2: $P < 0.0001$), no significant differences were observed between vaccinated and non-vaccinated control groups (H1N1: $P = 0.4118$; H3N2: $P = 0.2046$).

The relatively lower $CD8^+$ T cell response in vaccinated animals may account for the milder lesions observed in histopathological assessments. These animals displayed only mild alveolar septal thickening and limited interstitial inflammation, suggesting partial protection against severe lung damage. In contrast, non-vaccinated mice exhibited pronounced

pathological changes, including marked alveolar septal thickening, extensive lymphocytic infiltration, and proteinaceous exudates, indicative of severe lung injury. As expected, the normal saline group demonstrated preserved lung architecture and served as the healthy baseline. Overall, vaccination elicited a robust immune response that correlated with significantly reduced lung pathology. However, the comparatively lower $CD8^+$ T cell response in vaccinated mice may contribute to the observed attenuation in lung tissue damage (Figs. 8 and 9).

DISCUSSION

This study investigated the immunogenicity of a multi-epitope DNA vaccine designed to stimulate both humoral/cellular immunity and induce cross-protection against influenza A viruses (H1N1 and H3N2). The vaccine was developed using multiple epitopes from conserved and consensus regions of the H1H3 and PA proteins, employing an integrated approach that combined in silico predictions, in vitro validations, and in vivo evaluations. DNA vaccines are considered attractive alternatives to protein-based strategies due to their ease of manufacture and capacity to elicit both humoral and cell-mediated immune responses.

Using immunoinformatics tools, we designed a novel vaccine construct targeting epitopes from the PA and H1H3 (stem-overlapping) regions with high predicted binding affinity to MHC class I and II molecules and B cell receptors. These epitopes were selected for their broad protective potential against multiple strains of H1N1 and H3N2. Molecular docking confirmed the stability of interactions between the selected epitopes and immune receptors, predicting a stable and immunogenic construct with favorable physicochemical properties. To enhance immunogenicity and stability, the construct also incorporated appropriate adjuvants and linkers, as supported by docking results. In vitro validation through Western blotting confirmed expression of the vaccine construct, underscoring the accuracy of the in-silico design and supporting its translational potential. The demonstration of protein expression also served as a prerequisite for ethical approval to proceed to the in vivo phase.

In cytokine profiling, T-cell subset analysis and lung pathology assessments assays, no significant differences were found between the control groups injected with normal saline (NS) and empty plasmid (EP), evaluating them as appropriate negative controls. Post-vaccination, both Th1 and Th2 responses were induced. Elevated IFN-γ levels in vaccinated groups indicated strong cellular immune activation, reflecting the expansion of cytotoxic T lymphocytes (CTLs) essential for targeting influenza-infected cells. Additionally, elevated IL-4 levels in vaccinated animals confirmed robust B cell activation and a corresponding humoral response. Interestingly, non-vaccinated but challenged groups exhibited high IL-6 levels, suggesting heightened inflammation in the absence of vaccine-induced immunomodulation. This supports the conclusion that the vaccine reduced inflammation and lung damage in immunized groups (16). Across all challenged groups, elevated IL-10 levels suggested a general immune regulatory response, not specific to the vaccine. High early IL-10 levels are associated with enhanced viral replication, while elevated levels during later stages likely reflect the host's effort to limit tissue damage. Our findings are consistent with previous studies by Sun et al. (2009) and Wang et al. (2012), who highlighted the dual roles of IL-10 during infection (17-19).

Flow cytometry analysis revealed a notable increase in $CD8^+$ T cell populations in vaccinated groups, which correlated with elevated IFN-γ levels. In contrast, non-interventional control mice with more extensive lung lesions showed localized increases in $CD8^+$ cells in the lungs, likely as a response to severe infection. This difference reflects the effectiveness of PA epitopes in controlling viral replication and stimulating MHC class I–mediated responses. The critical role of PA epitopes was further supported by significantly reduced lung viral loads in vaccinated groups, as shown in Fig. 5F. This correlated with increased IFN-γ (Fig. 6B) and $CD8^+$ T cell responses (Fig. 8), indicating potent PA-specific cytotoxic activity.

An increase in $CD4^+$ T cell populations in the BAL and spleen confirmed MHC class II activation, supporting enhanced B cell responses and antibody production. Overall, a robust adaptive immune response was observed in vaccinated mice, as evidenced by elevated $TCD3^+$ cells in BAL and spleen samples. The presence of effector T cells in BAL fluid further demonstrated active immune cell recruitment to infection sites, essential for clearing infected cells and limiting viral spread in the respiratory tract. The

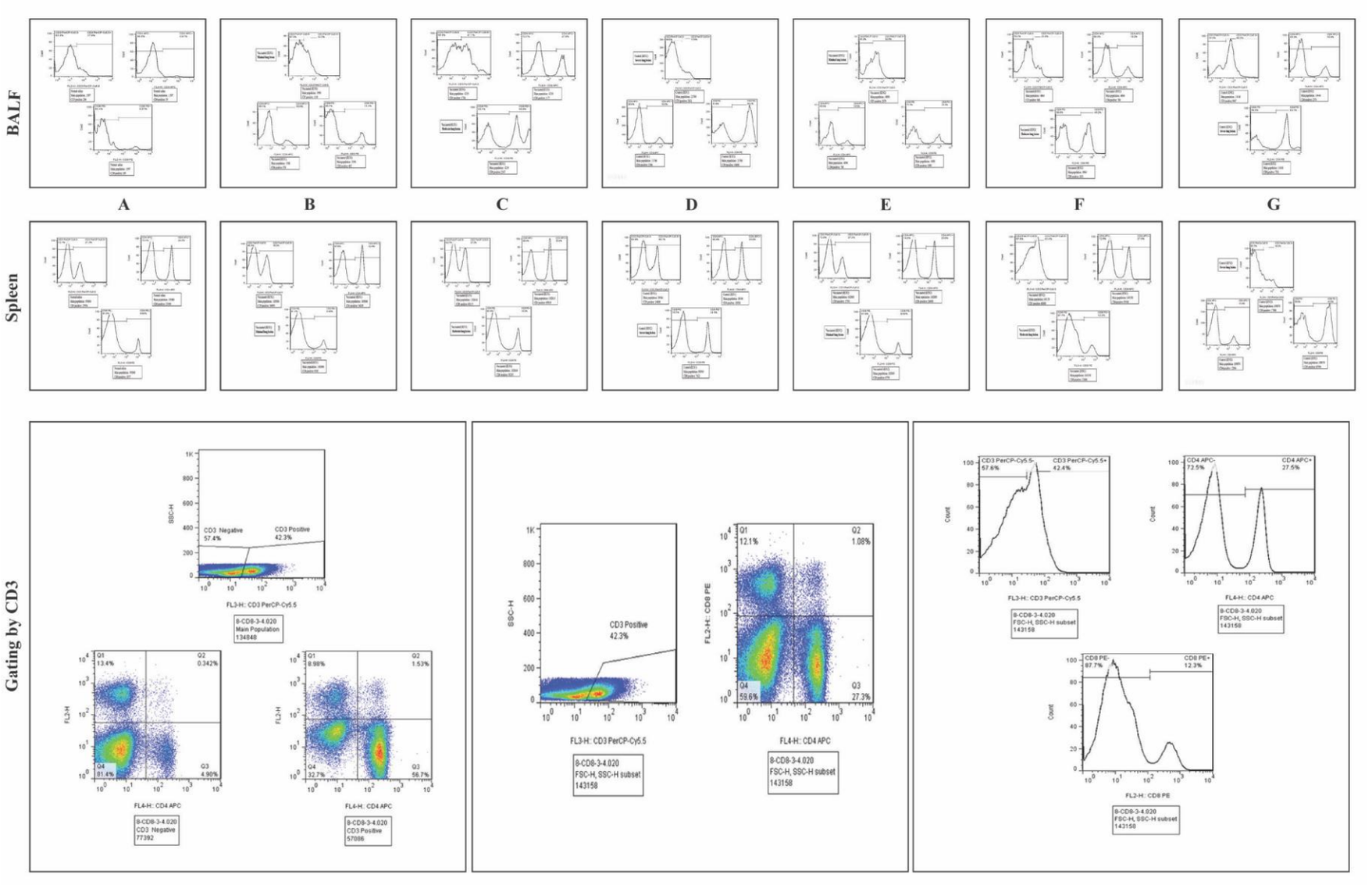
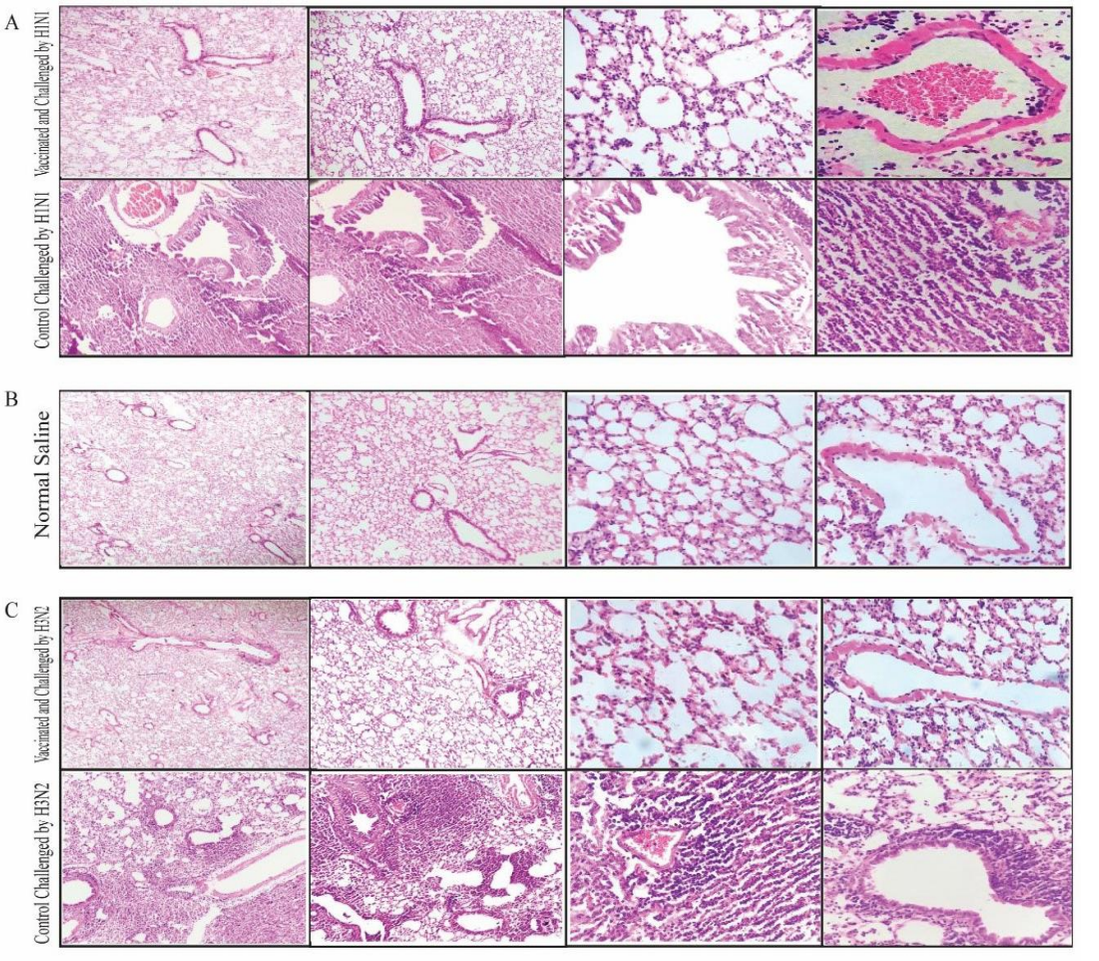


Fig. 8. 1-BALF and Spleen Flow Cytometry: Damage to the lungs by influenza viruses is considered part of the immunopathogenesis and is directly proportional to TCD8. In vaccinated groups, lung damage ranged from mild to moderate, whereas in non-vaccinated groups, severe lesions were observed. Flow cytometry gating by CD3: BALF and Spleen (A) Normal saline-injected (B) Vaccinated and challenged by H1N1 with minimal lung lesion (C) Vaccinated and challenged by H1N1 with moderate lung lesion (D) Non-vaccinated control challenged by H1N1 with severe lung lesion (E) Vaccinated and challenged by H3N2 with minimal lung lesion (F) Vaccinated and challenged by H3N2 with moderate lung lesion (G) Non-vaccinated control challenged by H3N2 with severe lung lesion. (8 mice per group).



D

Group	Alveolar septal thickening	Interstitial inflammation		Peribronchiolar lymphocytic infiltrate	Proteinaceous exudate alveolar lining cells	Alveolar lining cells hyperplasia	Desquamated alveolar lining cells
		PMN	Mononuclear cells (mostly lymphocytes)				
Vaccinated group challenged by H1N1	Mild< 10 %	none	Mild< 10 %	Minimal	Mild/none	Mild/none	Mild/none
Control group challenged by H1N1	Severe	Severe	Severe	Moderate	Severe	Moderate	Moderate
Normal Saline group	None	None	None	None	None	None	None
Vaccinated group challenged by H3N2	Minimal< 5 %	Minimal	Minimal	Minimal	None	None	None
Control group challenged by H3N2	Severe	Severe	Severe	Mild/ Moderate	Severe	Mild	Mild

Fig. 9. Pathology BALB/c Lung section staining by H and E method, (A) Vaccinated and control challenged by H1N1, vaccinated mice demonstrate well-preserved lung architecture accompanied by minimal inflammatory response. Control mice exhibit substantial alveolar thickening and notable inflammatory infiltration. (B) Normal saline (healthy lung tissue with a normal lung structure) (C) Vaccinated and control challenged by H3N2. The vaccinated group was challenged by H3N2 and displayed a moderate level of lung tissue preservation with diminished inflammation, whereas control mice exhibited extensive pulmonary damage and marked immune cell infiltration. (D) The analysis of lung pathology in BALB/c mice exposed to H1N1 and H3N2 viruses revealed that vaccinated groups had significantly less inflammation compared to control mice. In the H1N1 group, vaccinated mice showed mild changes, such as slight thickening of alveolar septa and minimal interstitial inflammation, while control mice had severe pathologies ($p < 0.01$). Also, the H3N2-challenged vaccinated group showed minimal changes, whereas control subjects suffered significant inflammation and tissue damage ($p < 0.01$). (8 mice per group).

vaccine platform promoted a diverse and regulatory population of $CD8^+$ memory T cells in the lungs, contributing to effective local immune responses and reducing the need for systemic T cell activation, as reflected in smaller spleen sizes in vaccinated animals. Influenza-specific T cells are crucial for infection control, as demonstrated by improved cytokine profiles and viral clearance in vaccinated mice (20-23). QRT-PCR analysis confirmed significantly lower viral loads in BAL fluids of vaccinated animals, highlighting the vaccine's efficacy in limiting viral replication and systemic dissemination.

Based on established immunological mechanisms, vaccination with the HA and PA epitopes used in this study induced IFN-γ-producing $CD8^+$ and $CD4^+$ T-cell responses, which may promote perforin- and granzyme-mediated killing of virus-infected cells, thereby reducing viral replication and limiting lung pathology (McKinstry et al., 2010; Iwasaki & Pillai, 2014) (24, 25). At the same time, HA-stem epitopes stimulate Th2 $CD4^+$ T cells, producing IL-4 to promote B-cell proliferation, class switching, and germinal center reactions, resulting in high-affinity HA-stem IgG antibodies. Although these stem-specific antibodies do not directly block receptor binding, they enhance viral neutralization by stabilizing HA in the pre-fusion conformation, preventing membrane fusion, and reducing the number of infected cells. These antibodies also mediate Fc-dependent effector functions, including ADCC via NK cells, which rapidly eliminate HA-expressing infected cells, and ADCP via macrophages and dendritic cells, which clear virions and apoptotic infected cells. Together, PA-induced cytotoxicity and HA-stem IgG–mediated Fc-effector mechanisms synergistically reduce viral replication and dissemination, resulting in strong in vivo protective immunity. These antiviral mechanisms are further supported by modulation of the cytokine environment. Early PA-specific T-cell–mediated viral clearance decreases activation of innate sensors such as RIG-I, MDA5, and TLR7, lowering IL-6 production and limiting inflammation and tissue damage (Hayashi et al., 2015; X Li et al., 2025) (26, 27). As infection resolves, regulatory T cells, M2-like macrophages, and tolerogenic dendritic cells produce IL-10, signaling through STAT3 to suppress excessive cytokine release and promote tissue repair (JM Rojas et al., 2017) (28). Meanwhile, IL-4 from Th2 cells supports B-cell maturation and optimal antibody responses. This integrated response, PA-targeted cytotoxic activity, HA-stem IgG with ADCC/ADCP, IFN-γ–driven cytotoxicity, IL-4–mediated humoral enhancement, and IL-10–mediated regulation, explains the observed reduction in viral load and lung lesions, and the establishment of a robust functional immune response.

Our findings are consistent with those of Lifang Yuan et al. (2024), who demonstrated that combining T and B cell epitopes enhances cross-protection for both H1N1 and H3N2 strains (29). However, unlike Kastenmüller et al (30), who reported increased total IgG levels, our study highlights the induction of highly functional antibodies, reflected by strong microneutralization titers even with modest total IgG levels. This suggests a more focused humoral response, potentially reducing the risk of antibody-dependent enhancement (ADE). Similarly, JZ Jia et al. (2024) emphasized that reduced total IgG does not necessarily indicate lower protection, reinforcing the role of high-affinity neutralizing antibodies in effective viral neutralization (31). Our results conclusively demonstrate the efficacy of the multi-epitope DNA vaccine in eliciting broad and robust immune protection against both H1N1 and H3N2 influenza A viruses in a BALB/c mouse model.

CONCLUSION

This study provides compelling evidence supporting the efficacy of a multi-epitope DNA vaccine based on conserved H1H3 and PA proteins in stimulating both humoral and cellular immune responses, thereby conferring cross-protection against influenza A viruses (H1N1 and H3N2) in a BALB/c model. Results from pathology, flow cytometry, and ELISA confirmed effective B and T cell interactions, reduced viral load in BAL fluid, and diminished lung inflammation and tissue damage in vaccinated groups. This innovative strategy represents a promising advancement in influenza vaccine development and offers potential for mitigating the morbidity and mortality associated with seasonal and pandemic influenza outbreaks.

ACKNOWLEDGEMENTS

This study was conducted as part of the PhD thesis of Khabat Barkhordari in Medical Virology at the

School of Public Health, Tehran University of Medical Sciences (TUMS). The authors gratefully acknowledge the staff of the Department of Medical Virology and the Influenza Center of the WHO located at the TUMS for their valuable technical assistance and support. We sincerely thank Dr. Nejati, Dr. Rad, Dr. Shahmahmudi, Dr. Mobini, and M. Mondeali for their kind help and assistance throughout this study.

REFERENCES

1. Paget J, Spreeuwenberg P, Charu V, Taylor RJ, Iuliano AD, Bresee J, et al. Global mortality associated with seasonal influenza epidemics: New burden estimates and predictors from the GLaMOR Project. *J Glob Health* 2019; 9: 020421.
2. Bedford T, Suchard MA, Lemey P, Dudas G, Gregory V, Hay AJ, et al. Integrating influenza antigenic dynamics with molecular evolution. Elife 2014; 3: e01914.
3. Lou J, Liang W, Cao L, Hu I, Zhao S, Chen Z, et al. Predictive evolutionary modelling for influenza virus by site-based dynamics of mutations. *Nat Commun* 2024; 15: 2546.
4. Shi W, Wohlwend J, Wu M, Barzilay R. Influenza vaccine strain selection with an AI-based evolutionary and antigenicity model. *Nat Med* 2025; 31: 3862-3870.
5. Yassine HM, Boyington JC, McTamney PM, Wei CJ, Kanekiyo M, Kong WP, et al. Hemagglutinin-stem nanoparticles generate heterosubtypic influenza protection. *Nat Med* 2015; 21: 1065-1070.
6. Krammer F, Palese P. Advances in the development of influenza virus vaccines. *Nat Rev Drug Discov* 2015; 14: 167-182.
7. Wei Y, Qiu T, Ai Y, Zhang Y, Xie J, Zhang D, et al. Advances of computational methods enhance the development of multi-epitope vaccines. *Brief Bioinform* 2024; 26(1): bbaf055.
8. Lu B, Lim JM, Yu B, Song S, Neeli P, Sobhani N, et al. The next-generation DNA vaccine platforms and delivery systems: advances, challenges and prospects. *Front Immunol* 2024; 15: 1332939.
9. Sidney J, Kim A-R, de Vries RD, Peters B, Meade PS, Krammer F, et al. Targets of influenza human T-cell response are mostly conserved in H5N1. *mBio* 2025; 16(2): e0347924.
10. Ooi A, Wong A, Esau L, Lemtiri-Chlieh F, Gehring C. A guide to transient expression of membrane proteins in HEK-293 cells for functional characterization. *Front Physiol* 2016; 7: 300.
11. Percie du Sert N, Hurst V, Ahluwalia A, Alam S, Avey MT, Baker M, et al. The ARRIVE guidelines 2.0: Updated guidelines for reporting animal research. *Br J Pharmacol* 2020; 177: 3617-3624.
12. Lequin RM. Enzyme immunoassay (EIA)/enzyme-linked immunosorbent assay (ELISA). *Clin Chem* 2005; 51: 2415-2418.
13. Cuevas F, Kawabata H, Krammer F, Carreño JM. An In Vitro Microneutralization Assay for Influenza Virus Serology. *Curr Protoc* 2022; 2(7): e465.
14. Fischer AH, Jacobson KA, Rose J, Zeller R. Hematoxylin and eosin staining of tissue and cell sections. *CSH Protoc* 2008; 2008: pdb.prot4986.
15. Kostinov M, Chuchalin A, Chebykina A, Khrapunova I, Cherdantsev A, Solov'eva I, et al. Clinical status and cytokine profiles in patients with asthma or chronic obstructive pulmonary disease vaccinated against influenza. *PLoS One* 2025; 20(2): e0313539.
16. Tang W, Xie H, Ye Z, Eick-Cost AA, Scheckelhoff M, Gustin CE, et al. Post-vaccination serum cytokines levels correlate with breakthrough influenza infections. *Sci Rep* 2023; 13: 1174.
17. Sun J, Madan R, Karp CL, Braciale TJ. Effector T cells control lung inflammation during acute influenza virus infection by producing IL-10. *Nat Med* 2009; 15: 277-284.
18. Wang SM, Tsai MH, Lei HY, Wang JR, Liu CC. The regulatory T cells in anti-influenza antibody response post influenza vaccination. *Hum Vaccin Immunother* 2012; 8: 1243-1249.
19. Couper KN, Blount DG, Riley EM. IL-10: the master regulator of immunity to infection. *J Immunol* 2008; 180: 5771-5777.
20. Zheng MZ, Fritzlar S, Wang Z, Tan TK, Kedzierska K, Townsend A, et al. Cutting edge: high-dose live attenuated influenza vaccines elicit pulmonary tissue-resident memory CD8+ T cells in the face of pre-existing humoral immunity. *J Immunol* 2022; 209: 1832-1836.
21. Zheng MZ, Tan TK, Villalon-Letelier F, Lau H, Deng YM, Fritzlar S, et al. Single-cycle influenza virus vaccine generates lung CD8+ Trm that cross-react against viral variants and subvert virus escape mutants. *Sci Adv* 2023; 9(36): eadg3469.
22. Del Campo J, Bouley J, Chevandier M, Rousset C, Haller M, Indalecio A, et al. OVX836 heptameric nucleoprotein vaccine generates lung tissue-resident memory CD8+ T-cells for cross-protection against influenza. *Front Immunol* 2021; 12: 678483.
23. van de Ven K, Lanfermeijer J, van Dijken H, Muramatsu H, Vilas Boas de Melo C, Lenz S, et al. A universal influenza mRNA vaccine candidate boosts T cell responses and reduces zoonotic influenza virus disease in ferrets. *Sci Adv* 2022; 8(50): eadc9937.
24. McKinstry KK, Strutt TM, Swain SL. Hallmarks of CD4 T cell immunity against influenza. *J Intern Med* 2011; 269(5): 507-518.

25. Iwasaki A, Pillai PS. Innate immunity to influenza virus infection. *Nat Rev Immunol* 2014; 14: 315-328.
26. Hu J, Ma C, Liu X. PA-X: a key regulator of influenza A virus pathogenicity and host immune responses. *Med Microbiol Immuno*l 2018; 207: 255-269.
27. Li X, Huang C, Rai KR, Xu Q. Innate immune role of IL-6 in influenza a virus pathogenesis. *Front Cell Infect Microbiol* 2025; 15: 1605446.
28. Rojas JM, Avia M, Martín V, Sevilla N. IL-10: a multifunctional cytokine in viral infections. *J Immunol Res* 2017; 2017: 6104054.
29. Yuan L, Zhang S, Bi R, Liu X, Han Z, Li M, et al. A broad-spectrum multiepitope vaccine against seasonal influenza A and B viruses in mice. *EBioMedicine* 2024; 106: 105269.
30. Haupt R, Baracco L, Harberts EM, Loganathan M, Kerstetter LJ, Krammer F, et al. Enhancing the protection of influenza virus vaccines with BECC TLR4 adjuvant in aged mice. *Sci Rep* 2023; 13: 715.
31. Jia JZ, Cohen CA, Gu H, McLean MR, Varadarajan R, Bhandari N, et al. Influenza antibody breadth and effector functions are immune correlates from acquisition of pandemic infection of children. *Nat Commun* 2024; 15: 3210.